Numerical investigation of heat transfer and fluid flow behavior around an oblate spheroid

I. Razgallah, Rafik Ouchene, Mohammed Khalij, Boris Arcen, Anne Tanière

NUMERICAL INVESTIGATION OF HEAT TRANSFER AND FLUID FLOW BEHAVIOR AROUND AN OBLATE SPHEROID

Intissar Razgallah[1], Rafik Ouchene[2]*., Mohamed Khalij[2]*, Borice Arcen[2]*, and Aanne Taniere[2]*

[1] *CNRS, ROBERVAL, UMR 7337, Université de Technologie de Compiègne*
Centre de Recherches de Royallieu CS 60319, 60203 Compiègne Cedex France
intissar.razgallah@utc.fr

[2] *CNRS, LEMTA, UMR 7563, Université de Lorraine – ESSTIN,*
2 rue Jean Lamour, 54500 Vandoeuvre-les-Nancy, France

mohammed.khalij@univ-lorraine.fr

Abstract

In this study, a numerical approach was adopted to investigate the heat transfer of an oblate spheroid in a steady flow of viscous and incompressible fluid characterized by Prandtl Numbers with values of 0.7, 1 and 7. The temperature of the spheroid is considered constant. This hypothesis is valid as the thermal conductivity of the particle is supposed to be much greater than the conductivity of the fluid. The uncoupled momentum and heat balance equations were solved numerically for particular Reynolds Numbers ranging from 0.1 to 100, corresponding to a laminar axisymmetric regime. Case studies were done on particles with aspect ratios of 0.2, 0.5 0.8 and 1. The validation of this work included a comparison of the numerical results of the drag coefficient, the local and the average Nusselt Numbers, to results found in literature and by visualization of the flow around the particle. The computations were focused on the influence of the axis ratios and the angle of attack on the heat transfer rate. It, also, shows the influence of the choice of the reference length of the spheroid, considered in the actual paper equal to the equivalent diameter of the sphere, on the variation of the Nusselt Numbers.

Keywords: Convection, heat transfer, oblate spheroid, sphere, aspect ratio, orientation, Nusselt number, drag coefficient, angle of attack

1. Introduction

Because of the inaccuracy produced by the sphericity assumption that was adopted in chemical engineering, scientists are keen to find more accurate shape assumptions to provide more reliable results in describing the flow and heat transfer around particles in industrial processes. These processes include combustion, chemical reactions, mixing and separation processes. Among these applications, oblate spheroidal shape seems to more precisely approximate the geometries in question and represent a good approximation for non-spherical particles [1]. Pulverized coal is for instance a good example to illustrate the products encountered [2,3]. In order to insure a better efficiency, it is of high interest to control with great accuracy such industrial processes through the knowledge of the settling velocity, which is greatly related to the drag forces, and the heat transfer coefficient usually determined by the Nusselt Number. A number of research papers have already treated the subject. However, limited attention was given to the effect of the emerged particle orientation on flow and heat transfer. Therefore, this will be the aim of this study. Thus, we express the orientation of the particle in terms of an angle of attack. Defined as the angle between the particle axis of revolution and the direction of flow, this angle was varied between 0° and 90° degrees.

2. Overview of the literature

We start this work by presenting an insight of the literature on unconfined spheroidal particles. Motion in creeping flow was first investigated by Stokes [4] on spherical particles. He developed the well-known expression for the drag coefficient by neglecting the inertial terms. Using the same approach, it was Oberbeeck [5], who started a similar work concerning ellipsoidal particles. Based on his results, Happel and Brenner [6] developed an expression for the drag coefficient by introducing an additional shape correction to the Stokes drag coefficient. Those shape correction factors, developed using an asymptotic method, also take the particle orientation into account. By determining the drag coefficient for the extreme angles of attack of 0° and 90°, a function linking these two limiting cases, with an inflection point at 45, can be used to represent the whole range of incidence angles for a non-spherical particle. As for spherical particles, the orientation has no effect on the motion of the particle. Therefore, the shape correction is constant and equal to 1.

For higher Reynolds Numbers a number of experimental and numerical studies were carried out in order to describe the drag coefficient in terms of Reynolds Numbers and the particle orientation. For the case of an ellipsoidal particle with an aspect ratio of 1, the particle is reduced to a sphere. The experimental study conducted by Schiller and Naumann [7] seems the most widely used correlation in this case. On the other hand, for an ellipsoidal particle most of the studies carried out are based on a numerical approach. Militzer et al. [8] used the existing data to develop a correlation describing the drag coefficient of a spheroid by introducing the aspect ratio into the Schiller and Naumann correlation [7]. The expression obtained is useful for particles of aspect ratios ranging between 0.2 and 5 and for Reynolds Numbers under 200. Unfortunately, this correlation doesn't take into account the orientation of the particle.

Stokes [4]	$C_D = \frac{24}{Re} : Re < 1,\ E=1$
Schiller and Naumann [7]	$C_D = \frac{24}{Re}\left(1 + 0.15\,Re^{0.687}\right) : Re < 700$

*LEMTA, CNRS.

Happel and Brenner [6]	$C_D = \frac{24\,K}{Re}$: E<1

With :

$$K(\alpha=0) = \frac{8E^{\frac{1}{3}}}{3\left[\frac{-E}{1-E^2}\frac{2E^2-3}{\left(E^2-1\right)^{3/2}}\sin^{-1}\sqrt{1-E^2}\right]}$$

$$K(\alpha=90) = \frac{8E^{-\frac{1}{3}}}{3\left[\frac{2E}{E^2-1}\frac{2(1-2E^2)}{\left(1-E^2\right)^{3/2}}\tan^{-1}\frac{\sqrt{E^2-1}}{E}\right]}$$

Other studies succeeded in taking the orientation of the particle into account. The most important ones are those conducted by Rosendhal [9], Zastawny et al.[10], Ouchene et al.[3], and Hölzer and Summerfeld[11]. The main difference between these correlations is the use of the parameters to describe the non-spherical shape of the particle and its orientation. Hölzer and Summerfeld used the sphericity and crosswise spherecity to characterize respectively these two parameters. Rosendhal, on the other hand, used first these two parameters to determine an expression of the drag coefficient at the extreme angles of attack. Then, he used a connecting function depending on the angle of attack. The rest of the studies were similar to Rosendhal's study except that they used the aspect ratio instead of the sphericity in establishing the correlations to describe the extreme values of the drag coefficient.

It was Fourrier [12], who first investigated a spherical particle placed in a surrounding fluid and gave an asymptotic expression for the Nusselt Number in a stagnant fluid. He proved that the diffusion is completely radial and results on a Nusselt Number equal to 2. More appropriate results in creeping flows were established by Brenner [13] who developed an analytical expression valid for small Peclet Numbers.

For infinite Peclet Numbers, Levich [14] used the thin boundary layer theory to develop an expression for the Nusselt Number that was enhanced later by Acrivos and Goddard [15] using a small perturbation method. However, Friedlander [16] was able to find a better expression.

Fourrier [12]	$Nu = 2$
Clift et al. [1]	$Nu = 1 + \left(1 + \mathrm{Re\,Pr}\right)^{1/3}$
Friedlander [16]	$Nu = \frac{4}{Pe} Ln\left(\frac{1}{1-\frac{Pe^2}{2}}\right)$
Brenner first order development [13]	$Nu_{2a} = Nu_0\left(1 + \frac{1}{8}Nu_0 Pe_{2a}\right)$
Brenner second order development [13]	$Nu_{2a} = Nu_0\left(1+\frac{1}{8}Nu_0\,Pe_{2a} + \frac{Nu_0}{16}\left(Pe_{2a}\right)^2 f_{0x} LN\left(Pe_{2a}\right)\right)$
Massliyah and Epstein [18]	$\mathrm{Nu}_{2a} = \frac{Nu_0}{2} + \left(\left(\frac{Nu_0}{2}\right)^3 + K^3\,Pe_{2a}\right)^{1/3}$

As for non-spherical particles, the diffusive heat transfer in a stagnant media was investigated by Smith, Weber and Schneider. Particularly, in the case of an oblate spheroid, the Nusselt Number expression depended on the orientation of the particle and was given for an angle of attack between 0° and 90°.

A valuable work was established in a Stokes flow regime by Brenner [13] using a matched asymptotic expansion method. The expression provided by him relies on the Nusselt Number in stagnant fluids and is adapted to arbitrary shapes. The orientation of the particle is taken into account by a dimensionless drag parameter defined as the ratio of the drag of an arbitrary shaped particle to the drag of the equivalent spherical particle.

Another expression by Sehlin [17] for heat and mass transfer from a spheroid particle was derived for infinit Peclet Numbers using the thin boundary layer theory. The established correlation is similar to Levich's expression modified using a concentration factor. Beside these analytical results, numerical studies on creeping flow were conducted by Massliyah and Epstein [18], Clift et al. [1] and Alassar [19].

For higher Reynolds Numbers, the heat transfer around a sphere was extensivly studied and a number of correlations were developed using expeimental and numerical approaches. The oldest are those established by Ranz and Marshall [20] and Whitaker [21]. Newer Correlations were then established by Clift et al. [1], Li and Mason [22], and Feng and Michailides [23] adapted for a wide range of Reynolds and Prandtl Numbers.

Ranz and Marshall [20]	$Nu = 2 + 0.6\,Re_p^{0.5}\,Pr^{1/3}$	0.6≤Pr≤400 4≤Re≤200
Whitaker [21]	$Nu = 2 + Pr^{0.4}\left[0.4\,Re_p^{0.5} + 0.06\,Re_p^{\frac{2}{3}}\right](\frac{\eta}{\eta_{wall}})^{1/4}$	1 ≤Re≤ 105
Clift et al. [1]	$Nu = 1 + (1 + Re_p\,Pr)^{1/3}$	$0 \le Re \le 1$
	$Nu = 1 + Re_p^{0.41}\,(1 + \frac{1}{Re_p\,Pr})^{1/3} Pr^{1/3}$	$1 \le Re \le 100$
	$Nu = 1 + 0.752\,Re_p^{0.472}\,(1 + \frac{1}{Re_p\,Pr})^{1/3} Pr^{1/3}$	$100 \le Re \le 200$
Li and Mason [22]	$Nu = 2 + 0.6\,Re_p^{0.5}\,Pr^{1/3}$	$0 \le Re \le 200$

	$Nu = 2 + 0.5{Re_p}^{0.5} Pr^{1/3} + 0.02{Re_p}^{0.8} Pr^{1/3}$	$200 \leq Re \leq 1500$
	$Nu = 2 + 0.000045\, {Re_p}^{1.8}$	$Re > 1500$
Feng and Michailides [23]	$Nu = 0.852\, \mathrm{Pe}^{\frac{1}{3}}(1 + 0.233\ {Re_p}^{0.287}) + 1.3 - 0.182{Re_p}^{0.355}$	$1 \leq Re \leq 500$ $1 \leq Pe \leq 1000$
Richter and Nikrityuk [2]	$Nu = 1.7 + 0.568 Pr^{\frac{1}{3}}\sqrt{Re} + 0.0104 Pr^{\frac{1}{3}} Re^{\frac{2}{3}}$	$10 \leq Re \leq 200$ Pr=0.74

In the case of ellipsoidal particles, few correlations had been established for particles with a flat orientation including the studies by Comer and Kleinstreuer [24], by Clift et al. [1] and by Srinivas and Ramesh [25].

α=0°

Author	Correlation	Domain
Comer and Kleinstreuer [24]	$Nu_{2a} = 1.393\, Re_{2a}^{0.348} \exp[0.248\,(1-E)]$ Pr=0.7	$40 \leq Re_{2a} \leq 120$ $0.2 \leq E \leq 1$
	$Nu_{2a} = 2.074\, Re_{2a}^{0.415} \exp[0.31\,(1-E)]$ Pr=7	
Clift et al. [1]	$\frac{Nu_{2a} - \frac{Nu_0}{2}}{Nu_{E=1} - 1} = \frac{1.25}{1 + 0.25\, E^{0.9}}$	$1 \leq Re_{2a} \leq 100$ $0.2 \leq E \leq 5$
Srinivas and Ramesh [25]	$\frac{Nu_{2a,\ E\neq 1}}{Nu_{E=1}} = 1.2917\, Exp(-0.256\, E)$	$0 \leq Re_{2a} \leq 100$ $1 \leq Pr \leq 100$ $0.5 \leq E \leq 2$ $0.4 \leq n \leq 1.6$
Richter and Nikrityuk [2]	$Nu_{de} = 1.59 + 0.64 Pr^{\frac{1}{3}}\sqrt{Re_{de}} - 0.039 Pr^{\frac{1}{3}} Re_{de}^{2/3}$	$10 \leq Re_p \leq 250$ Pr=0.74 E=2

α=90°

Author	Correlation	Domain
Kishore and Gu [26]	$Nu_{2b} = 2E^{0.3} + Pr^{0.4}[0.4\, Re_{2b}^{0.5}\, E^{0.83} + 0.06 Re_{2b}^{2/3}\, E^{0.1}\ ]$	$1 \leq Re_{2b} \leq 200$ $1 \leq Pr \leq 1000$ $0.25 \leq E \leq 2.5$
Sreenivasulu et al. [27]	$Nu_{2b} = 2E^{0.3} + Pr^{0.37}[0.77\, Re_{2b}^{\frac{0.755}{n+1.31}}\, E^{0.07} + 0.02 Re_{2b}^{1.05}\, E^{0.63}\ ]$	$5 \leq Re_{2b} \leq 100$ $5 \leq Pr \leq 100$ $0.5 \leq E \leq 1.5$ $0.5 \leq n \leq 1.5$

These correlations are valid on a small range of Peclet Numbers. For a 90° angle the only correlations known were developed by Kishore and Gu [26] and Sreenivasulu et al. [27] As the first correlation has a wide range of validity, it seemed less accurate at hight Prandtl Numbers compared to the correlation established by Sreenivasulu et al. with a maximum relative error reaching 28% between their numerical results and the correlation. On the other hand, the correlation by Sreenivasulu et al. seems to cover only Prandtl Numbers larger than 5.

Thus we need more accurate correlations for these extreme angles. Since there seems to be no published research that investigates the effect of intermediate angles on heat transfer we have run a numerical study to investigate this effect and try to find a correlation which takes this aspect into account.

3. Problem formulation and governing equations

In this work, a solid oblate spheroid of constant temperature T_s is immerged in a homogeneous unbounded Newtonian fluid. With constant properties, the velocity fluid field is independent of its temperature field. We consider that the conductivity of the particle is very important compared to the conductivity of the fluid which allow us to suppose an instant homogenization of the temperature of the particle on its surface. The fluid is supposed to have a uniform velocity U_0 far from the particle. Its temperature is maintained constant T_∞ and lower than T_s, with $|T_s - T_\infty|$=100K. Since, in this paper, we use only small Mach numbers, we can consider the fluid as being incompressible.

Its density is thus constant and we can neglect buoyancy effects. The object is of length '2a' in the direction normal to flow and '2b' in the direction parallel to flow called the major and minor axes respectively. Characterizing an oblate spheroidal shape, the aspect ratio is defined as the ratio of the ellipsoidal minor to major radius E = (b/a), ranges between 0 and 1 for an oblate spheroid. If E tends to 0, the particle considered is a flat circular disk. Whereas, if E=1 the particle is identical to a sphere. In this study, we will examine the cases for E=1, E=0.8, E=0.5 and E=0.2 (fig.1).

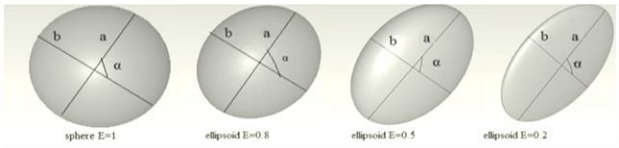

Fig. 1 : Scheme of investigated particles

The heat transfer process is governed by the conservation equations.

$$div\,(\vec{u}_f) = 0 \tag{1}$$

$$\frac{D\vec{u}_f}{Dt} = -\frac{1}{\rho_f}\,grad\,p_f + \mu\Delta\vec{u}_f + \vec{g} \tag{2}$$

$$\frac{\partial T_f}{\partial t} = \vec{u}_f\,\overrightarrow{grad}(\,T_f) + K_f\,\Delta\,T_f \tag{3}$$

Those equations are converted into dimensionless form using the equivalent diameter as a reference length, U_0 as a reference velocity and as a temperature scale $T* = \frac{T - T\infty}{Ts - T\infty}$.

$$div\,(\overrightarrow{u*}) = 0 \tag{4}$$

$$\frac{D\vec{u}*}{Dt} = -grad\,p* + \frac{1}{\mathrm{Re}}\nabla^2\vec{u}* \tag{5}$$

$$\frac{DT*}{Dt} = \frac{1}{Re\,Pr}\,\nabla^2\,T* \tag{6}$$

Where Reynolds and Prandtl numbers are dimensionless groups deduced from the non-dimensional form of the equations.

The boundary conditions are specified in fig. 2. The usual boundary conditions are the no slip conditions on the body and the free stream conditions far away from the body.

4. Simulation

Using FLUENT 15.0, the equations of conservation (eqn (1), eqn (2) and eqn (3)) were solved for a certain number of cases. The different cases simulated are given in table 1. For this purpose, we used the SIMPLE algorithm for Pressure-Velocity Coupling that suits unstructured meshes. The domain is chosen to have a cuboid form. It is schematized on fig.2. Consisted of tetrahedral elements, our mesh is sufficiently refined near the surface of the particle using the method of gradual inflation and captures the dynamic boundary layer by a minimum of 40 nodes (fig. 3). As for spatial discretisation, it was done using a second order upwind scheme.

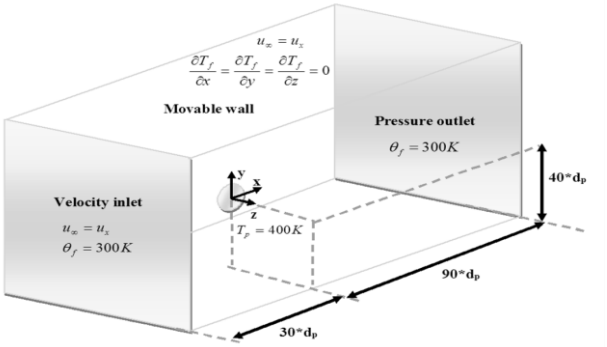

Fig. 2 : Domain of computation and boundary conditions

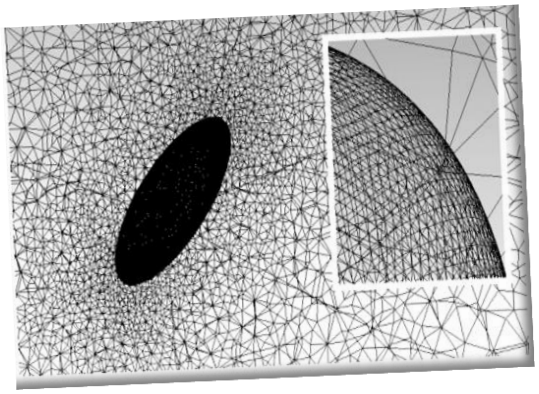

Fig. 3 : Used grid

Table 1 : Parameters of simulation

Aspect ratio E	Reynolds number Re	Prandtl number Pr	Angle of attack α	Equiv. diameter d_e
1	0.1, 1, 10, 60,100	0.7, 1, 7	0°	1
0.2, 0.5, 0.8	0.1, 1, 10, 20, 40, 60, 80, 100	0.7, 1, 7	0° et 90°	1.1696, 1.5874, 1.8566
0.2, 0.5, 0.8	1, 60, 100	0.7, 1, 7	15°,30°,45°,60°,75°	1.1696, 1.5874, 1.8566

4.1. Validation of the simulation results

Before analysing the results of the present work it is important to make sure the correctness of the numerical scheme. First, we asserted that the dimensions of the domain are sufficiently large enough in order to insure that the fluid at the boundaries is not influenced by the walls. On the other hand, it should be as small as possible to reduce the calculation time. For

this purpose, we tested three dimensions (table 2). Knowing that the boundary layer is thicker as the Reynolds number is smaller, the drag coefficient was compared for the different domain dimensions considering a Reynolds number equal 0.1. We notice that we get a sufficient result for a domain with a length equal 40 $d_{p.}$

Table 2 : Domain validation

Re=0.1	
Diameter of the domain by particle diameter $\frac{D}{d_p}$	Drag coefficient C_D
40	247.40
60	245.43
80	245.09

It is also important to ensure a sufficient number of nodes in the area near the surface of the particle, where the velocity and temperature gradients are the greatest. For this purpose we compared the results obtained for average Nusselt number and drag coefficient obtained for three grids with different nodal numbers. In table 3, we notice that we receive sufficient results with grid A. There is only an error smaller than 1% between Grid A and Grid C if we compare the Nusselt Number obtained for each case. So we fixed the number of nodes for all the simulated cases *to the same number imposed by grid A.*

Table 3 : Grid validation

Re=100, Pr=7 and α=90			
		C_D	Nu
Grid A	739749	1.126	12.483
Grid B	993488	1.122	12.529
Grid C	3039817	1.119	12.556

4.2. Comparison in the case of the sphere

In this section we discuss the different results obtained during the simulation and we compare them to the results found in the literature. A comparison in table 4 of the drag coefficient obtained by simulation and the results by Stokes and by Schiller and Naumann [7] was possible for a Reynolds of 0.1. It shows a relative error of 1% between our results and those by Schiller and Naumann [7] and a 3% of relative error between our results and those by Stokes [4]. This is mostly due to the fact that the relation by Stokes was neglecting the friction at small Reynolds numbers.

Table 4 : Comparison of drag coefficient in creeping flow

Re=0.1			
	Actual	Stokes [4]	Schiller and Naumann [7]
C_D	247.60	240	247.40

For higher Reynolds numbers, the comparison was only possible for the results from the equation of Schiller and Naumann [7] (Fig. 4). Here, we obtained again a good accuracy with 4% as a maximum error, and an average relative error of 1.9%.

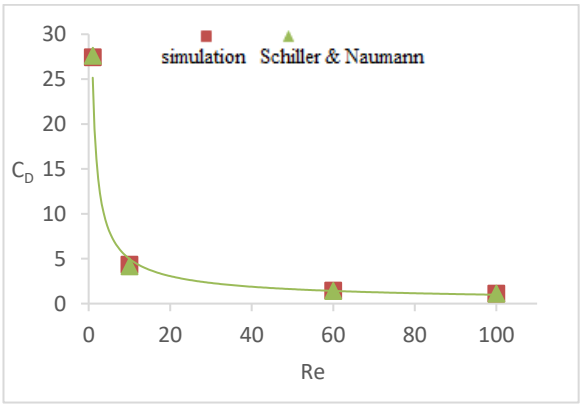

Fig.4 : Comparison of drag coefficient for high Reynolds numbers

The average Nusselt number is defined in spherical coordinates as shown in eqn (7), where Nu_ϕ is the local Nusselt number and Nu, is the average Nusselt number. The calculations were done with an equivalent diameter equal to the sphere diameter.

$$Nu = \frac{1}{360}\int_0^{180} Nu_\phi \sin\phi \, d\phi \tag{7}$$

The local Nusselt number is defined by eqn(8)

$$Nu_\phi = \frac{-\left.\frac{\partial T_f}{\partial n}\right|_{paroi}}{\left(\frac{T_s - T_\infty}{\phi}\right)} \tag{8}$$

In order to verify the results obtained for heat transfer, we chose to compare the results of the Nusselt average obtained numerically, for Reynolds at 0.1 in a creeping flow and different Prandtl numbers, to results from Fourrier [12], Clift et al. [1] and Friedlander [16]. As shown in table 5, our numerical results are close to the asymptotic solution by Fourier [12]. The relative error between our results and those of Friedlander increases up as the Peclet number become larger than 0.1. In that case, the conduction is dominating. The correlation by Clift et al. [1] shows smallest error to ours with a maximal relative error of 1.7%.

Table 5 : Comparison of average Nusselt number in creeping flow for Reynolds of 0.1

	Nu			
Pr	Numerical	Fourrier [12]	Clift et al. [1]	Friedlander [16]
0.7	2.030	2	2.023	2.035
1	2.043	2	2.032	2.051
7	2.231	2	2.193	2.461

Another way of validating the results is done by making sure that we really capture the thermal and dynamic boundary layer. For a Peclet number of 1, the dynamic and thermal boundary layers are mingled and the thickness of the boundary layer is equal to y=13.08 dp. This is of course largely contained on the

domain that we chose. To verify the evolution of the thermal boundary layer in terms of Prandtl number, for a fixed Reynolds number of 1, fig. 5 shows the evolution of non-dimensional temperature variation on the vertical plane. The results obtained show that the thickness grows when the Prandtl number gets smaller and verify the relation:

$$\frac{\delta_T}{\delta} \cong \mathrm{Pr}^{-1/3} \; si \; \mathrm{Pr} > 1 \; quand \; 0{,}6 \le \mathrm{Pr} \le 50$$

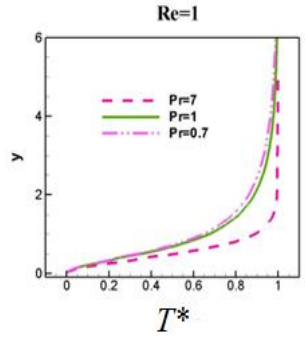

Fig. 5 : Thermal boundary layer for a Reynolds of 1 and different Prandtl number

Since the convective heat transfer coefficient varies over the surface of the sphere, we expect the Nusselt number to vary locally. This variation is mainly influenced by the flow regime of the fluid that surrounds it. In Fig. 6, the variation of local Nusselt number is plotted dependent on the polar angle expressed here in Radian for a Reynolds of 0.1, and for the different values of the Prandt number studied. The local Nusselt number increases as the number of Prandtl becomes larger. This is due to the fact that the convective heat transfer rises as Prandtl increases. Moreover, we note that the curve have a maximum at the breakpoint level. Following which the local Nusselt number decreases gradually as one moves away from the stop point downstream of the obstacle. This decrease is due to the fact that the boundary layer becomes less dense.

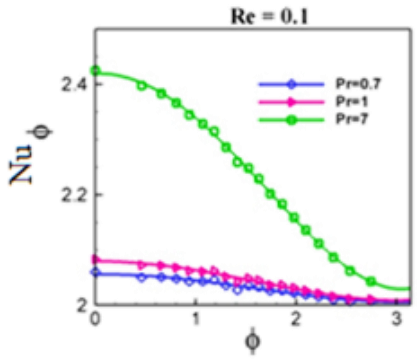

Fig. 6 : Local nusselt number distribution for Reynolds of 0.1 and different Prandtl number.

For high and intermediate Reynolds numbers, a comparison of our numerical results was possible with the results by Feng and Michailides [23], Clift et al. [1], Comer and Kleinstreuer [24], Li and Mason [22], Whitaker [21] and Richter and Nikrityuk [2] (fig. 7). For all the Prandtl numbers considered, excellent compatibility was found between our simulation results and the correlation established by Feng and Michailides [23] as well as those established by Clift et al. [1] (table 6). However, the latter appears to underestimate the results for Pr = 7 when the Reynolds number is greater than 60 with a maximum relative deviation equal to 4.4%. The correlations of Comer and Kleinstreuer [24] for a Prandtl numbers of 7 and 0.7, seems to describe with good accuracy the average Nusselt number for a Reynolds number greater than 10. As for the correlations of Li and Mason [22] and Whitaker [21], they seem to underestimate or overestimate the average Nusselt number especially for high Reynolds number. For a Prandtl number of 0.7, the correlation by Richter and Nikrityuk [2] seems best suited with a maximum relative error of 1.4% regardless of the Reynolds considered between 1 and 100. At large Prandtl numbers, strong convective currents yielded increased Nusselt numbers.

As for the local Nusselt number, its evolution in terms of the polar angle was schematized in fig.8 for each Reynolds number and Prandtl number studied. The first thing that comes to mind is the increase of local heat transfer when Reynolds or Prandtl are large. From the comparison of our results with the results of Massliyah and Epstein [18] or those of Juncu [28] we get a perfect match. For a Reynolds number of 100, it is clearly detected, see fig.8, the occurrence of a minimum of the local Nusselt number for which the polar ϕ angle is 2.5 radians. This angle corresponds to the point of flow separation. We notice, also, that starting from a polar angle of 1.57 radians, corresponding to 90 degrees, the Nusselt number falls and reaches an almost constant value regardless of the Reynolds number. In order to check the behavior of the boundary layer in the vicinity of the particle, we have plotted the variation of the thickness of the boundary layer in this area as a function of Reynolds number (fig. 9).

The variation of the thermal boundary layer is proportional to $\frac{1}{\sqrt{\mathrm{Re}^{0,5}}}$ and to $\frac{1}{\mathrm{Pr}^{1/3}}$ as it is the case for a flat plate.

5. Results for a spheroid and discussion

Unlike a sphere, an oblate spheroid can be characterized by different equivalent lengths. In this study, we considered the equivalent length to be the principal axis of the spheroid. In order to compare the different results in literature, it is practical to observe the relations given in eqn(9)

$$\begin{aligned} d_e &= 2b\ E^{2/3} = 2a\ E^{-1/3} \\ Re_{de} &= Re_{2a} E^{1/3} \\ Nu_{de} &= Nu_{2a} E^{1/3} \end{aligned} \qquad (9)$$

A comparison of the numerically obtained drag coefficient was possible to the analytical expression of the drag coefficient developed by Happel and Brenner [6]. The results are compiled in Table 7 for a Reynolds number of 0.1 and for different aspect ratios. This comparison is made for an angle of attack of 0° and 90°. Note that the drag coefficient increases with increasing aspect ratio. There is a maximum of 5% relative difference between numerical and theoretical results. This discrepancy is due to negligence in formulating Happel and Brenner [6] inertial terms.

To validate the numerical results obtained by solving the energy equation, we proceed to compare the change in the local Nusselt number with the results out of the literature. It is the study by Massliyah and Epstein [18], which appears to be the first of

its kind to have attached importance to the understanding of the mechanism that rules the local heat transfer on the surface of ellipsoidal particles. The authors were able to characterize, through a numerical study, the heat and mass transfer around a spheroidal particle having an aspect ratio of 0.2 for a range of intermediate Reynolds up to 100 and a Prandtl number of 0.7. As for the average heat transfer, they proposed correlations for the average Nusselt number that cannot be used easily due to the complexity of the equivalent length they chose. Indeed, they adopted as equivalent length, the perimeter of the sphere of the same contour as the particle. Following this article, another article by Comer and Kleinstreuer [24] treated the same subject by considering solid ellipsoids and oblate droplets with an aspect ratio ranging between 0.2 and 1 for a range of intermediate Reynolds numbers ranking between 40 and 120 while the considered Prandtl numbers are 0.7 and 7. Finally, a qualitative study by Juncu [28], described the local heat transfer in axisymmetric steady flow before studying the transitional regime. Two cases were considered. When the heat capacity of the particle is large enough, the temperature is assumed to be constant as it is the case in this study. Otherwise, a spatial variation of the temperature is taken into account. The latter study is conducted on particles of oblate and prolate shape with an aspect ratio ranging between 0.1 and 0.9 in a range of Reynolds number of 10 and 100. The Prandt number is kept equal to 1 and 10. The comparison shows a match between our simulation results and those of Juncu [28], Comer and Kleinstreuer [24] and Massliyah and Epstein [18]. Generally, for a fixed Reynolds and a fixed orientation, the local Nusselt number increases with Prandtl. In addition, the variation of the local Nusselt is not monotonic [25]. We note that for an aspect ratio of 0.8, the variation of the local Nusselt number is similar to the case of the sphere to the extent that both admit a maximum at the front stagnation point corresponding to a zero φ. Then, as the aspect ratio decreases, the maximum shifts. This phenomenon is analogous to the reduction of viscous friction when the aspect ratio decreases [24]. The local Nusselt number exhibited a large value at the front stagnation point and then decreased till the point of separation and then again increased towards the rear stagnation point.

On the other hand, similar to the case of the sphere, the minimum local Nusselt number is observed at the point of separation for the different aspect ratios considered. This observation is clearly visible at higher Peclet number (Fig. 10). By comparing the shape of the plots, with an aspect ratio of 0.2, Renolds of 2 and 100, and Prandtl of 0.7 and 10, note that the separation becomes very visible at large Prandtl numbers. The point of separation away from the stopping point as the aspect ratio increases. And downstream of the point of separation, the local Nusselt number is increasing which is not the case when no separation occurs. In this area, the local Nusselt number is almost independent of the aspect ratio. The fore-aft symmetry is present in the oblate case at very small Reynolds numbers only. This asymmetry leads to wake formation and augments the convective currents resulting in enhanced heat transfer coefficients for intermediate Reynolds numbers.

On another hand, the comparison of our numerical results of the average Nusselt number in a creeping flow shows a good agreement with the results obtained by Brenner [13] in his first order development of the average Nusselt number especially for small Peclet numbers. For this purpose, we had to convert the results obtained from the latter expression to be expressed in terms of equivalent diameter (table 8). With an average error of 1.48%, this relationship takes the geometry shape into account through the aspect ratio but has no consideration of the orientation of the particle. To estimate the precision of the numerical results we obtained for different attack angle, we compared those results at 0° and 90° to the second order development of Brenner [13] valid for an aspect ratio of 0.2 (table 9). The results obtained show that the effect of the orientation increase as the Peclet number become larger. This relation overestimate the average Nusselt number for higher Prandtl numbers and underestimate it at small Prandtl numbers. For aspect ratios different than 0.2 (table 10), the relation given by Massliyah and Epstein [18] yields betters results. The accuracy of the average Nusselt number increases when the aspect ratio rises.

For average Reynolds numbers and particle with a null orientation angle, a series of comparisons is presented on fig.11. The correlation by clift et al., Srinivas and Ramesh [25] and Comer and Kleinstreuer [24] give reliable results when Prandtl number is equal to 0.7 and 1. Those correlations are suitable for any aspect ratio. However, for a greater Prandtl number, the first two correlations yield poor results while the third authors relations, defined only for specific prandtl numbers of 0.7 and 7, are suitable. In that last case, the results are showing a maximum error of 8% on the domain of Reynolds numbers ranging between 10 and 100. The observations from the comparison with clift et al. [1] and Srinivas and Ramesh [25], are in agreement with the validity domains of the correlations. In fact, they are valid for Pe_{2a} numbers inferior to 100, Where Pe2a is the Peclet number with equivalent length defined as the great axe of the spheroid. This limit is already reached for a Reynolds number of 10 and a Prandtl number equal to 7 for a small aspect ratio of 0.2. However for a bigger aspect ratio, this limit is not reached yet. The lack of more precise correlations with a larger domain of validity is shown. As for an orientation of 90°(voir fig.12), comparison was only possible with Kishore and Gu [26] and Sreenivasulu et al. [27]. The first authors, developed an expression which underestimates the average Nusselt number. In fact, even if their correlation was valid in a wide range of Reynolds and Prandtl, it seems less precise than the expression developed by Sreenivasulu et al. especially at higher Reynolds numbers where the maximum error reaches 25% for an aspect ratio of 0.5. The maximum error, according to the researchers can even reach 28%. The relative error diminishes as the aspect ratio gets larger and reaches an average value of 10% for an aspect ratio of 0.8. On the other hand, the mathematical equation developed by Sreenivasulu et al. is only valid for a Prandtl number higher than 5. The comparison shows a good fit between the simulation results and the correlation with a maximal error of 10% in the range of Reynolds numbers between 10 and 100. The precision grows with the Reynolds number and the aspect ratios growth. However, unfortunately, no correlation exists to evaluate the heat transfer around a spheroid with an aspect ratio of 0.2.

The variation of the average Nusselt number is proven to increase with the Reynolds number and the Prandtl number for any aspect ratio considered (fig.13 and fig.14). In order to understand the effect of the aspect ratio on the variation of heat transfer, we fixed Reynolds and Prandtl and we plotted the average Nusselt number depending on the aspect ratio (fig.15). The variation of the Nusselt number depending on the aspect ratio follows a growing non-linear evolution for an orientation of 0° or 90°. A non-monotonic variation is observed in particular for an orientation of 0°. However, if the Nusselt number is recalculated using the major axis of the particle, the variation becomes monotonous (fig. 16). And the more important is the aspect ratio, the more important is the heat transfer if we consider the

equivalent length to be the major axis of the oblate spheroid. In case the equivalent length is the minor axis, we get the opposite variation. This aspect shows the importance of the equivalent length on the variation of the Nusselt number.

In order to investigate the effect of the variation of the intermediate angles of attack, we show in fig. 17 the variation of the Average Nusselt number with an equivalent length equal to the major axis, Reynolds of 100 and Prandtl of 7, expressed in terms of the aspect ratio. The figure shows a monotonous variation. It is maximal at 0° and decreases as the angle of attack increases.

6. Conclusion

A numerical study on heat transfer characteristics has been carried over spheroidal shaped body immersed in a Newtonian incompressible fluid. The ranges of parameters studied consist of a wide range of Reynolds and Prandtl numbers. It was observed that average heat transfer variation over a spheroid depends on the equivalent length we choose. The flow separation that takes place in the oblate spheroid case at Reynolds numbers as low as 30 at 0° orientation is responsible for them having a larger Nusselt number when Reynolds is higher. This flow separation coupled with large Prandtl numbers can yield very high heat transfer coefficients for the oblate spheroids. The variation of heat transfer in terms of orientation of the particle in the fluid is proved to increase when the attack angle is higher. In further works, we will try to develop a simple correlation that one can use to predict the Nusselt number over spheroidal shaped bodies in a wide range of Nusselt and Prandtl numbers. This correlation should also be valid for the case of the sphere.

References

[1] Clift, R., Grace, J. & Weber, M. Bubbles, Drops and Particles. Academic Press, New York, 1978.

[2] Richter, A. & Nikrityuk, P. New correlations for heat and fluid flow past ellipsoidal and cubic. Powder Technology, Volume 249, p. 463–474, 2013.

[3] Ouchène, R., Khalij, M., tanière, A. & Arcen, B. Drag lift and torque coefficients of the ellipsoidal particles. C. F., s.n., 2013.

[4] Stokes., G. On the effect of the inertial friction of fluids on the motion of pendulums. s.l.:Trans. Cambridge Phil. Soc., 1851.

[5] Oberbeek, A. Ueber stationäre Flüssigkeitsbewegungen mit Berücksichtigung. J Reine Angew Math, 81, p. 62–80, 1876.

[6] Happel, J. & Brenner, H. Low Reynolds Number Hydrodynamics. Prentice-Hall, Englewood Cliffs, 1965.

[7] Schiller, A. & Naumann, L. A drag coefficient correlation. VV.D.I. Zeitung, Volume 77, p. 318–320, 1935

[8] Militzer, J., Kan, J., Hamdullahpur, F., Amyotte, P., & Taweel, A. Drag coefficient for axisymmetric flow around individual sphéroidal particles. Powder Technology, 57, p. 193-195, 1989.

[9] Rosendahl, L. Using a multi-parameter particle shape description to predict the motion of non-spherical particle shapes in swirling flow. Appl. Mathematical Modelling, p. 11–25, 2000

[10] Zastawny, M., Mallouppas, G., Zhao, F. & Van Wachem, B. Derivation of drag and lift force and torque coefficients for non-spherical particles in flows. International Journal of Multiphase Flow. Int. J. Multiphase Flow, p. 288–295, 2012.

[11] Hölzer, A. & Sommerfeld, M. New simple correlation formula for the drag coefficient of non-spherical particles. Powder Technology, Volume 184, p. 361–365, 2008.

[12] Fourier, J. Theorie Analytique de la Chaleur. s.l.:Paris, 1822.

[13] Brenner, H. Forced convection heat and mass transfer at small Péclet numbers from a particle of arbitrary shape. Chemical Engineering Science, 18(London), p. 109-122, 1963.

[14] Levich, V. G., & Technica, S. *Physicochemical hydrodynamics* (Vol. 689). Englewood Cliffs, NJ: Prentice-hall. 1962.

[15] Acrivos, A. & Goddard, J. D. Asymptotic expansions for laminar forced-convection heat and mass transfer. Journal of Fluid Mechanics, 23(02), pp. 273- 291, 1965.

[16] Friedlander, S. Mass and heat transfer to single spheres and cylinders at low Reynolds numbers. AIChE J. 3, p. 43–48, 1957.

[17] sehlin, R. C. M. Forced convection heat and mass transfer at large Peclet numbers from axisymmetric body in laminar flow: prolate and oblate spheroids, Pittsburgh, Pennsylvania: Carnegie-Mellon Univ of technology, 1969.

[18] Masliyah, J. & Epstein, N. Numerical solution of heat and mass transfer from spheroids in steady axi-symmetric flow. Prog. Heat Mass Transfer, Volume 6, p. 613–632, 1972.

[19] Alassar, R.S. Forced convection past an oblate spheroid at low Reynolds numbers. J. Heat Transf., 127. 2005, p. 1062-1070, 2005.

[20] Ranz, W. & Marshall, W. Evaporation from drops. Chem. Eng. Proc., 48, p. 173–180, 1952.

[21] Whitaker, S. Forced convection heat transfer correlations for flow in pipes, past flat plates, single cylinders, single spheres, and for flow in packed beds and tube bundles. AIChE J. 18, p. 361–371, 1972.

[22] Li, J. & Mason, D. A computational investigation of transient heat transfer in pneumatic transport of granular particles. Powder Technology, 112, p. 273-282, 2000.

[23] Feng, Z. G. & Michaelides, E. M. Heat and mass transfer coefficients of viscous sphere. International journal of Heat and Mass Transfer, Volume 44, p. 4445-4454, 2001.

[24] Comer, J. & Kleinstreuer, C. Computational analysis of convection heat transfer to non-spherical particles. Int. J. Heat Mass Transfer, Volume 38, p. 3171–3180, 1995.

[25] Srinivas, B. & Ramesh, K. V. Numerical analysis of Heat Transfer from a Spheroidal Shaped Body to a Power Law Fluid at Finite Reynolds Number. CFD letters, Volume 6(1), 2014.

[26] Kishore, N. & Gu, S. Momentum and heat transfer phenomena of spheroid particles at moderate Reynolds and

Prandtl numbers. International Journal of Heat and Mass Transfer, Volume 54, p. 2595-2601, 2011.

[27] Sreenivasulu, B., Srinivas, B. & Ramesh, K. Forced convection heat transfer from a spheroid to a power law fluid. International Journal of Heat and Mass Transfer, Issue 70, p. 71–80, 2014.

[28] Juncu, G. Unsteady heat transfer from an oblate/prolate spheroid, *International Journal of Heat and Mass Transfer*, vol. 53, p. 3483-3494, 2010.

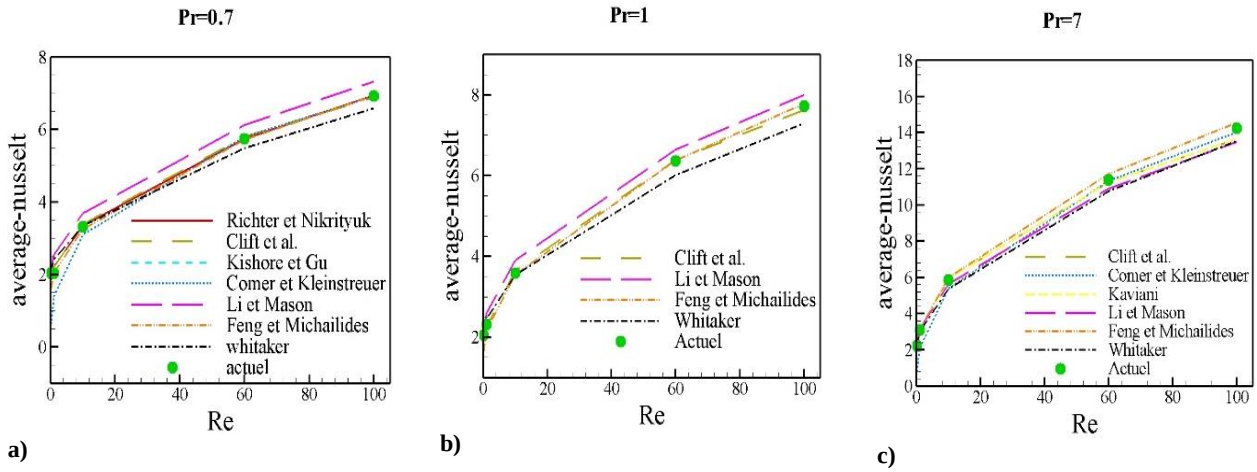

Fig. 7 : Comaprison of average Nusselt number for a sphere at high Reynolds number for a) Prandt number = 0.7 b) Prandt = 1 c) Prandt = 7

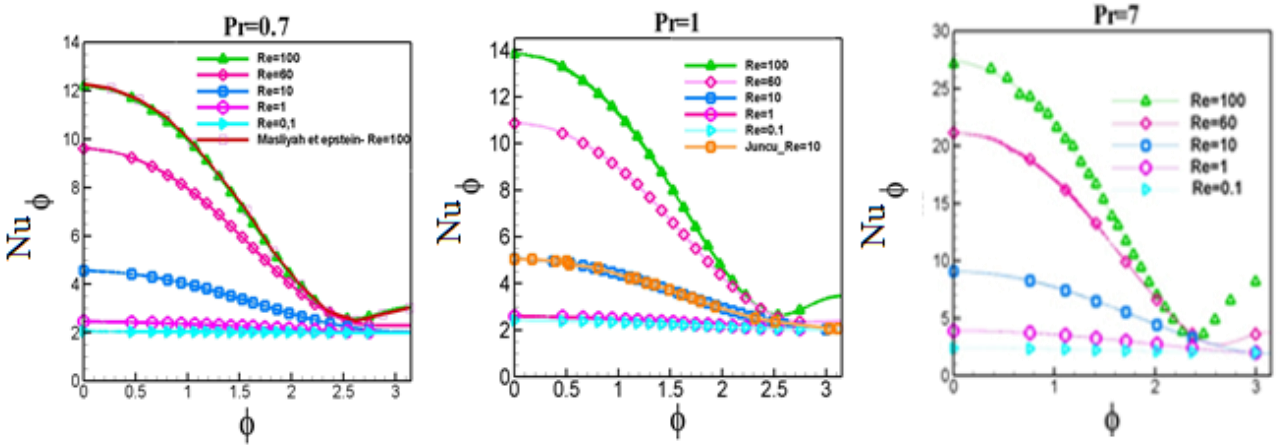

Fig. 8 : Variation of local Nusselt number for different Reynolds number and Prandtl number in the case of the sphere

Table 6 : Average and maximum relative error between our numerical results of the average Nusselt number and some correlations out of the literature for the case of the sphere

correlation	Validity domain	Average relatif error (%)	Maximum relatif error (%)
Feng and Michailides [23]	1<Rep<500 et 1<Pe<1000	1,3	7.03
Clift et al. [1]	$0<Re_p<100$	1,65	4.39
Whitaker [21]	$1<Re_p<100$	4,72	9.13
Li and Mason [22]	$0<Re_p<100$	6,27	11.35

Table 7 : Comparison of the drag coefficient in the case of oblate spheroid for Reynolds of 0.1 with different aspect ratio and orientation

	C_D			
Orientation α	90°		0°	
E	Actual	Happel and Brenner [6]	Actual	Happel and Brenner [6]

0.2	281.752	279.068	372.153	353.534
0.5	245.558	235.857	287.762	273.654
0.8	249.919	232.678	237.168	248.190
Average relative error	2.59%		4.95%	

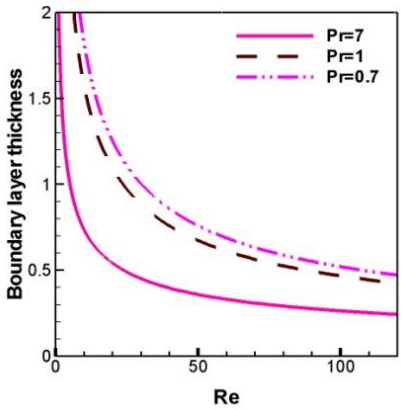

Fig. 9 : thermal boundary layer variation with Reynolds number for different Prandtl number

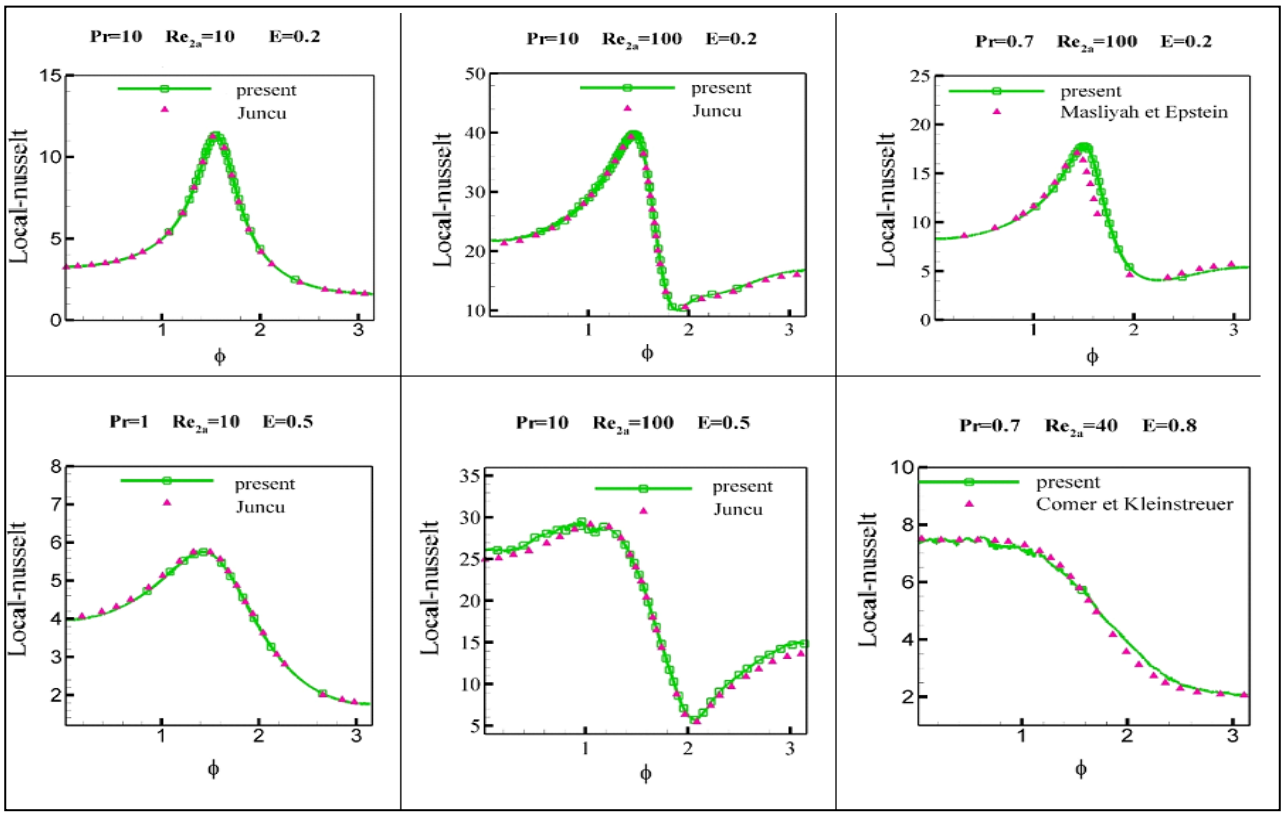

Fig. 10 : Comparaison of the variation of local Nusselt number on the surface of the oblate particle at zero attaque angle for different Reynolds Prandtl and E

Table 8 : Comparison of the numerical results of average Nusselt number for a spheroid of aspect ratio of 0.2, 0.5 and 0.8 and a Prandtl number of 0.7,1and 7 at creeping flow with a Reynolds number equal to 0.1

E		
0.2	0.5	0.8

Average Nusselt number		Actual	Brenner (1st order) [13]	Actual	Brenner (1order) [13]	Actual	Brenner (1 order) [13]
Pr	0.7	1.559	1.549	1.931	1.918	2.017	2.003
	1	1.571	1.557	1.945	1.925	2.032	2.008
	7	1.730	1.721	2.129	2.062	2.207	2.118
Relative error		0.68%		1.61%		1.96%	

Table 9 : Comparison of the numerical results of average Nusselt number for a spheroid of aspect ratio of 0.2 at different orientations and Prandtl numbers at creeping flow with a Reynolds number equal to 0.1

E = 0.2	Orientation α			
	0°		90°	
Pr	Actual	Brenner (2d order) [13]	Actual	Brenner(2d order) [13]
0.7	1.559	1.5451	1.559	1.543
1	1.571	1.5503	1.571	1.546
7	1.7308	1.7576	1.742	1.775
Average relative error	1.26%		1.5%	

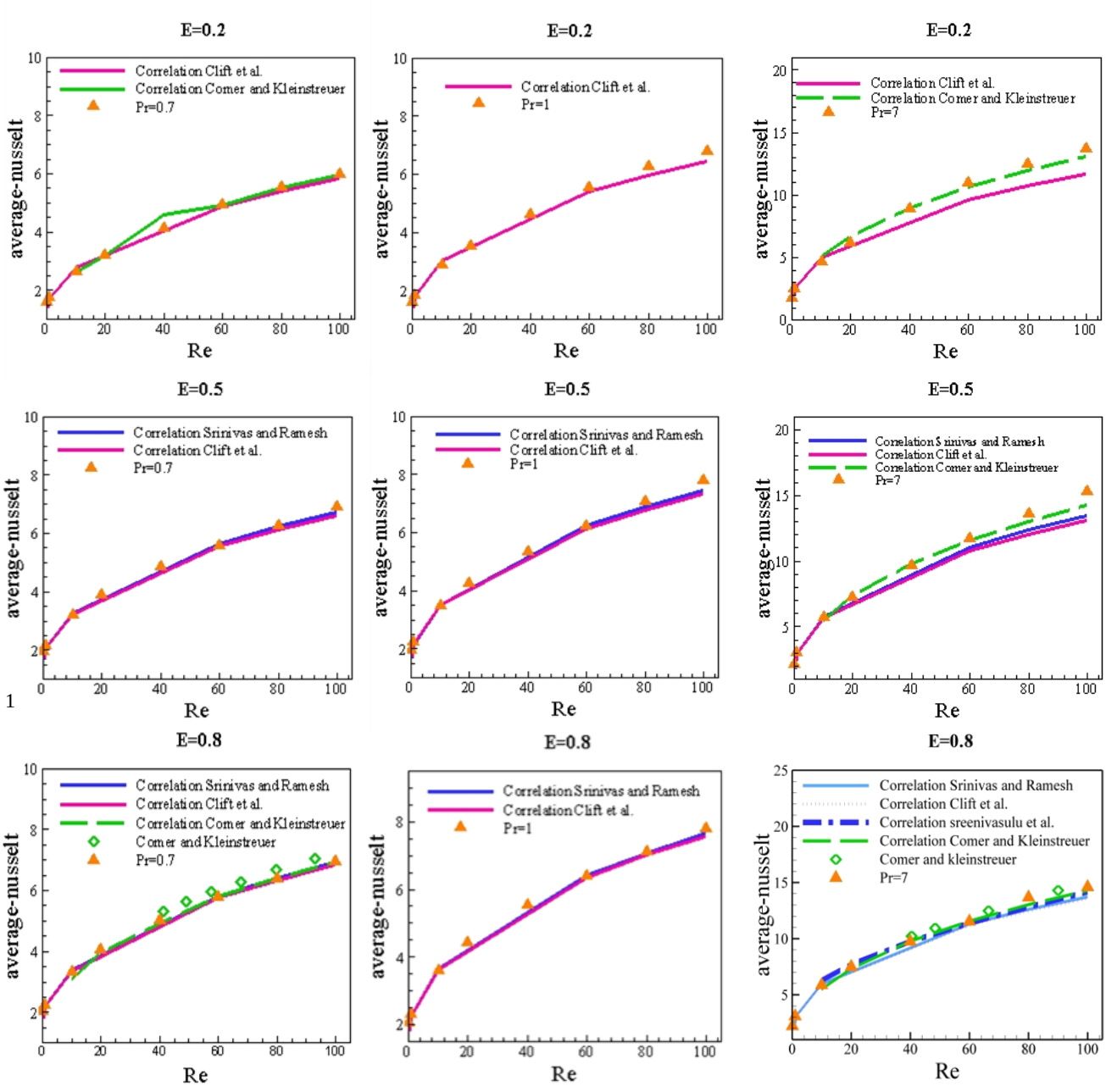

Fig. 11 : Comparision of average Nusselt number for an orientation of 0° at high and intermediate Reynolds numbers.

Table 10 : Comparison of the numerical results of average Nusselt number for a spheroid of different aspect ratios and Prandtl numbers at creeping flow with a Reynolds number equal to 0.1

	E					
	0.2		0.5		0.8	
Pr	Actual	Massliyah and Epstein [18]	Actual	Massliyah and Epstein [18]	Actual	Massliyah and Epstein [18]
0.7	1.559	1.547	1.932	1.923	2.017	2.011
1	1.571	1.554	1.945	1.932	2.032	2.02
7	1.731	1.673	2.129	2.082	2.207	2.171
Average error	1.73%		1.11%		0.84%	

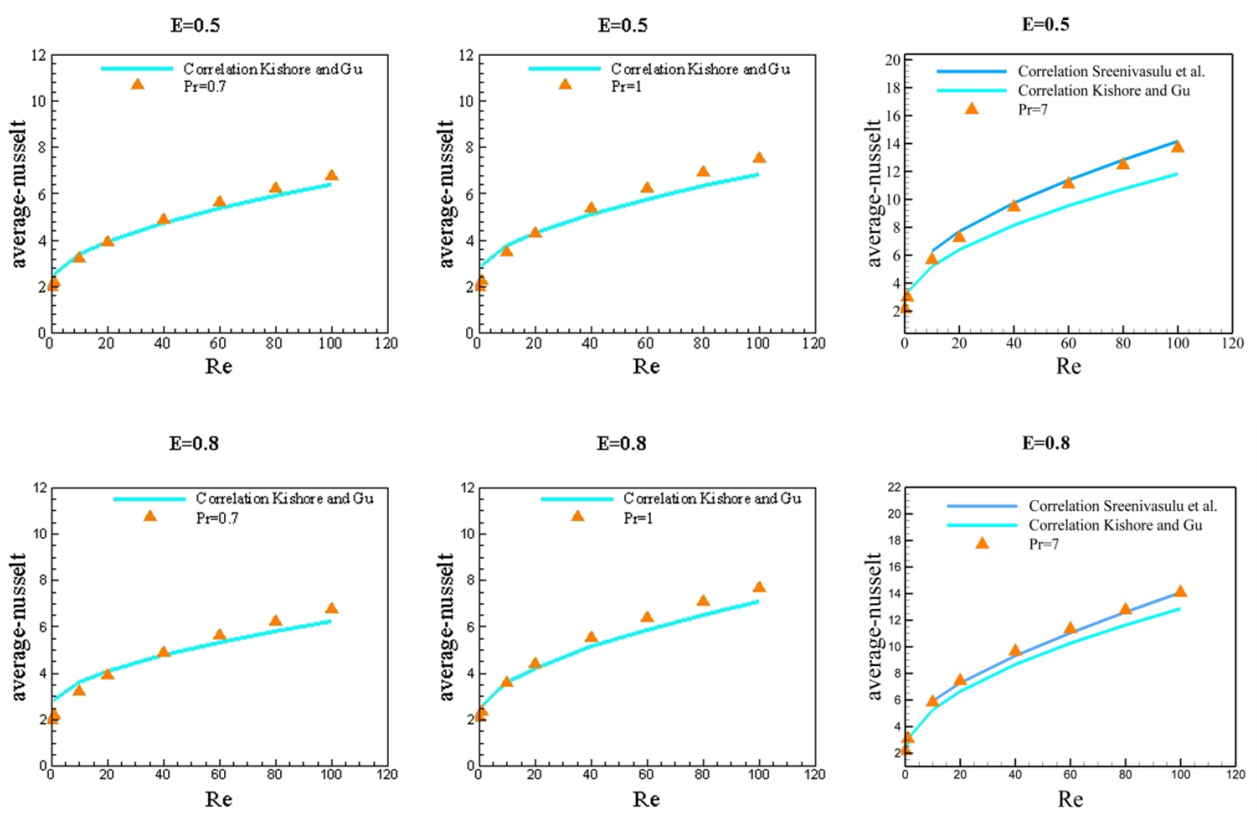

Fig. 12 : Comparison of average Nusselt number for an orientation of 90° at high and intermediate Reynolds numbers.

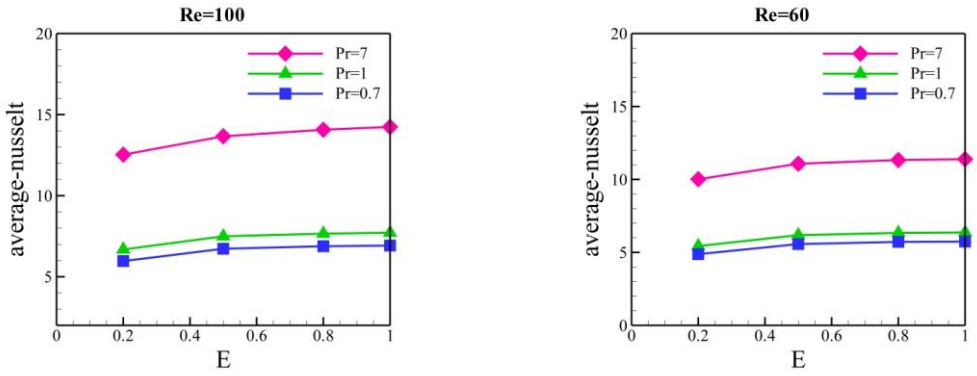

Fig. 13 : Variation of the average Nusselt number in terms of aspect ratio for an angle of attack of 90° at fixed Reynolds numbers

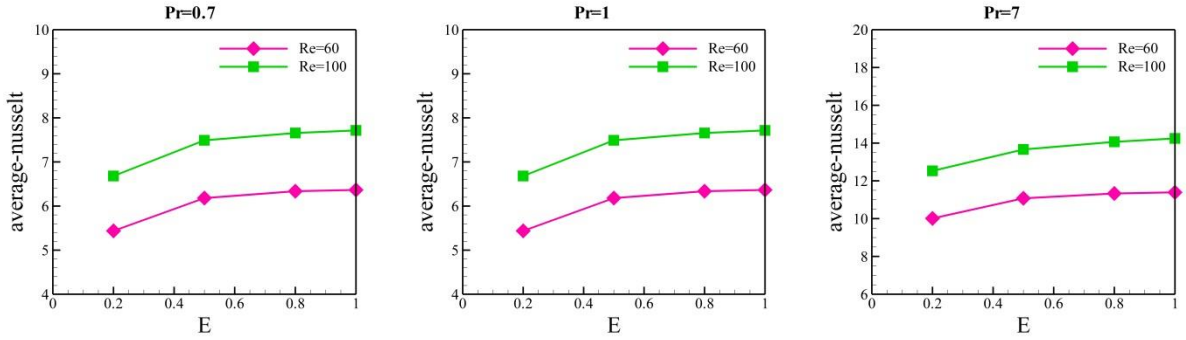

Fig. 14 : Variation of the average Nusselt number in terms of aspect ratio for an angle of attack of 90° at fixed Prandtl numbers

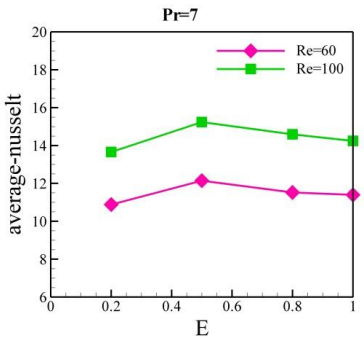

Fig. 15 : Variation of the average Nusselt number in terms of aspect ratio for an angle of attack of 0° at fixed Prandtl number

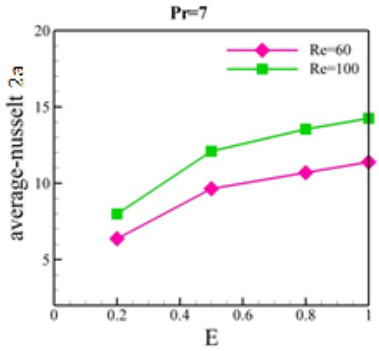

Fig. 16 : Variation of the average Nusselt number having an equivalent length equal to the major axis of the spheroid number in terms of aspect ratio for an angle of attack of 0° at fixed Prandtl number

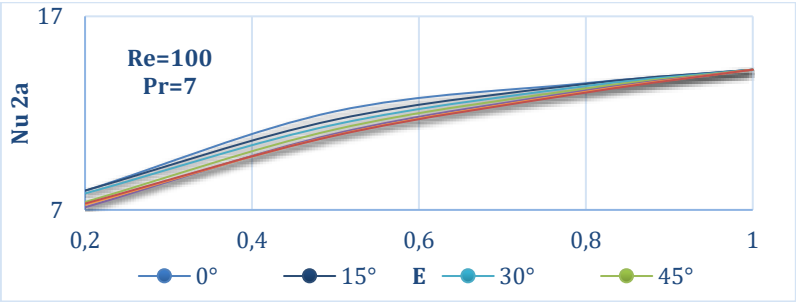

Fig. 17 : Variation of the average Nusselt number having an equivalent length equal to the major axis of the spheroid number in terms of aspect ratio for the different angles of orientation at fixed Prandtl numbers.